Chinese Journal of Chemical Engineering 55 (2023) 293–303

Contents lists available at ScienceDirect

Chinese Journal of Chemical Engineering

journal homepage: www.elsevier.com/locate/CJChE

Full Length Article

Probing deactivation by coking in catalyst pellets for dry reforming of methane using a pore network model

Yu Wang #, Qunfeng Zhang #, Xinlei Liu, Junqi Weng, Guanghua Ye *, Xinggui Zhou

State Key Laboratory of Chemical Engineering, School of Chemical Engineering, East China University of Science and Technology, Shanghai 200237, China

ARTICLE INFO

Article history:
Received 10 January 2022
Received in revised form 10 April 2022
Accepted 9 May 2022
Available online 13 June 2022

Keywords:
Deactivation by coking
Dry reforming of methane
Pore network model
Diffusion limitation
Catalyst pellet

ABSTRACT

Dry reforming of methane (DRM) is an attractive technology for utilizing the greenhouse gases (CO_2 and CH_4) to produce syngas. However, the catalyst pellets for DRM are heavily plagued by deactivation by coking, which prevents this technology from commercialization. In this work, a pore network model is developed to probe the catalyst deactivation by coking in a Ni/Al_2O_3 catalyst pellet for DRM. The reaction conditions can significantly change the coking rate and then affect the catalyst deactivation. The catalyst lifetime is higher under lower temperature, pressure, and CH_4/CO_2 molar ratio, but the maximum coke content in a catalyst pellet is independent of these reaction conditions. The catalyst pellet with larger pore diameter, narrower pore size distribution and higher pore connectivity is more robust against catalyst deactivation by coking, as the pores in this pellet are more difficult to be plugged or inaccessible. The maximum coke content is also higher for narrower pore size distribution and higher pore connectivity, as the number of inaccessible pores is lower. Besides, the catalyst pellet radius only slightly affects the coke content, although the diffusion limitation increases with the pellet radius. These results should serve to guide the rational design of robust DRM catalyst pellets against deactivation by coking.

1. Introduction

The large consumption of fossil fuels, *e.g.*, coal, oil, and natural gas, has led to the elevated level of CO_2 in the atmosphere, which causes global warming. To meet this grand challenge, extensive efforts have been devoted to developing technologies for carbon capture, storage and utilization (CCSU) [1–3]. Dry reforming of methane (DRM) is one attractive technology for CO_2 utilization, as it takes two abundant greenhouse gases, namely CO_2 and CH_4, as raw materials to produce economically valuable syngas [4–6] (see Eq. (1)). The syngas produced from DRM has a H_2/CO ratio less than or close to 1 due to the reverse water gas shift (RWGS) reaction [5] (see Eq. (2)). This syngas is very suitable for the synthesis processes where high CO fraction is required, such as the production of dimethyl ether and high-carbon alcohols [7,8].

$$CH_4 + CO_2 \rightleftharpoons 2CO + 2H_2 \qquad \Delta H_{298\,K} = +247\ \text{kJ}\cdot\text{mol}^{-1} \tag{1}$$

$$CO_2 + H_2 \rightleftharpoons CO + H_2O \qquad \Delta H_{298\,K} = +41.2\ \text{kJ}\cdot\text{mol}^{-1} \tag{2}$$

To develop an economically feasible DRM process, an efficient and stable catalyst is required. Since DRM reaction is strongly endothermic and its reactants are relatively inert, a reaction temperature higher than 916 K is needed to achieve a reasonable reaction rate [9]. However, under such high temperature, coking reactions, including methane cracking, carbon monoxide disproportionation, and carbon monoxide hydrogenation [10] (see Eqs. (3)–(5)), become important in affecting the performance of DRM catalysts. Coke may cover active sites, reduce pore volume of a catalyst support, and even break a catalyst pellet, which results in catalyst deactivation and pulverization [11–15]. Extensive experiments on DRM have confirmed that DRM catalysts are vulnerable to coke deposition. For example, Sokolov *et al.* [16] prepared DRM catalysts with Ni metal supported on TiO_2 and Al_2O_3, and they found the activities of Ni/TiO_2 and Ni/Al_2O_3 catalysts decrease by 89% and 20% after testing the catalysts for 100 h. Kim *et al.* [17] reported that 47% (mass) of coke was formed in a Ni/Al_2O_3 catalyst prepared by the co-precipitation method after 1 h on stream, and the catalyst was significantly deactivated due to pore plugging by coke.

$$CH_4 \rightarrow C + 2H_2 \qquad \Delta H_{298\ K} = +75\ \text{kJ}\cdot\text{mol}^{-1} \tag{3}$$

$$2CO \rightarrow C + CO_2 \qquad \Delta H_{298\ K} = -172\ \text{kJ}\cdot\text{mol}^{-1} \tag{4}$$

* Corresponding author.
E-mail address: guanghuaye@ecust.edu.cn (G. Ye).
# These authors contributed equally to this work.

https://doi.org/10.1016/j.cjche.2022.05.015
1004-9541/

$$CO + H_2 \rightarrow C + H_2O \qquad \Delta H_{298\ K} = -175\ \text{kJ} \cdot \text{mol}^{-1} \tag{5}$$

Some works have been carried out to develop a DRM catalyst with high robustness against deactivation by coking. These efforts [17–20] primarily focus on designing active sites that can effectively catalyze DRM reaction but inhibit coking reactions. However, few works pay attention to designing pore network structure of DRM catalyst pellets, which should also be very effective in reducing catalyst deactivation by coking. A well design of pore network can enhance the capacity to contain coke and reduce the diffusion resistance caused by coke deposition. For instance, Keil and Rieckmann [21,22] studied the deactivation of hydrodemetallization catalysts, and they found that the catalyst with a high pore coordination number has a longer lifetime. Ye *et al.* [23,24] probed the deactivation by coking of a Pt-Sn/Al_2O_3 catalyst for propane dehydrogenation, and they found pore network structure can significantly affect catalyst lifetime and apparent activity.

To aid the design of pore network in DRM catalyst pellets, a proper mathematical model is needed. This model should be able to describe the dynamic change of pore network structure during catalyst deactivation by coking. Continuum and pore network models are available to simulate deactivation by coking in catalyst pellets. Continuum models [25] are simple and efficient, but cannot describe pore blockage caused by coking. Pore network models can well describe the morphology and topology of pore space in catalyst pellets, and thus these models are suitable for simulating catalyst deactivation by coke deposition. Besides, pore network models have been successfully used to simulate catalyst deactivation in hydrodemetalation [22], Claus reaction [26], and propane dehydrogenation [23,24], where pore blockage occurs. Thus, a pore network model is suitable to investigate deactivation by coking in DRM catalyst pellets, and this model has not yet been developed up to now.

In this work, we develop a pore network to simulate deactivation by coke deposition in DRM catalyst pellets. This pore network model is able to describe the detailed pore network structure, including spatial distribution of pore size and pore connectivity, and to combine the equations for diffusion, reaction, coking, and deactivation. Using this model, the deactivation by coking in DRM catalyst pellets is probed, and the effects of reaction conditions and pore network structure on the catalyst deactivation are obtained.

2. Modeling

A Ni/Al_2O_3 catalyst pellet commonly used in DRM reaction is taken as the model catalyst when building the pore network model in this work. The pore network model is composed of three parts: pore network, equations for reaction and diffusion, and equations for coke deposition. A three-dimensional pore network established by connecting pores and nodes is a well representation of the real catalyst pellet. In each pore, diffusion, reaction, and coke deposition occur, and the equations for these processes are tightly coupled. By solving these equations, the concentration profiles and pore states can be achieved. In the calculations, the pore network structure is changed with the progress of coking, and the pore network structure should be updated according to the distribution of coke loading.

2.1. Pore network construction

DRM catalyst pellets can be assumed to be spherical as this pellet shape is widely used in the industry. The spherical pore network can be constructed by using the method reported in our previous work [23,24,26]. This method is briefly described as follows. Firstly, a cubic pore network is built by connecting nearest nodes with pores according to pore connectivity. Then, this cubic pore network is cut into a spherical pore network by using the pore network cutting algorithm [27]. Finally, pore diameter is assigned to each pore. In this work, the pore diameter follows the logarithmic normal distribution [28]:

$$p(\frac{d_0}{2}) = \frac{V}{\sigma \frac{d_0}{2}\sqrt{2\pi}} e^{-\frac{\left(\ln\frac{d_0}{2} - \ln\frac{d_a}{2}\right)^2}{2\sigma^2}} \tag{6}$$

Here, d_0 is the pore diameter, V is the total pore volume of the DRM catalyst pellet, σ is the standard deviation of pore diameter, and d_a is the volume-averaged pore diameter. Fig. 1 displays a typical, spherical pore network with a pore connectivity of 6. In addition, the nodes are normally treated as zero-volume intersections, and all the pore volume is occupied by pores. It is worth noting that pellet shape can change diffusion path length, and then affect the diffusion in a catalyst pellet [29–31]. Thus, the effect of pellet shape should be similar to that of pellet size, which is investigated in this work.

2.2. Equations for reaction and diffusion

The mass balance equation is applied to describe the coupled diffusion and reaction process for component i at each pore n:

$$\frac{\partial C_{i,n}}{\partial t} = -\frac{\partial J_{i,n}}{\partial l_n} + \frac{4d_{0,n}}{d_{p,n}^2} R_{i,n} \tag{7}$$

Here, $C_{i,n}$ is the molar concentration of component i in pore n, t is time, $J_{i,n}$ is the diffusion flux of component i in pore n, l_n is the length of pore n, $d_{0,n}$ is the initial diameter of pore n, $d_{p,n}$ is the real-time diameter of pore n, and $R_{i,n}$ is the reaction rate of component i in pore n. The quasi-steady-state condition is assumed since coking rate is much slower than the rates of diffusion and reaction, and Eq. (7) can be changed into:

$$0 = -\frac{dJ_{i,n}}{dl_n} + \frac{4d_{0,n}}{d_{p,n}^2} R_{i,n} \tag{8}$$

For an inner node, due to its zero-volume assumption, the mass balance equation for component i is:

$$\sum_{n=1}^{n=Z} \frac{\pi d_{p,n}^2}{4} J_{i,n} = 0 \tag{9}$$

where Z is the pore connectivity. For a boundary node, a Robin boundary condition is adopted:

$$-k_i(C_{i,b} - C_{i,n}) = J_{i,n} \tag{10}$$

where k_i is the mass transfer coefficient of component i on the external surface of the catalyst pellet, $C_{i,b}$ is the concentration of component i in the bulk, and $C_{i,n}$ is the concentration of component i in the pore n that is connected to the boundary node. The mass transfer coefficient of component i (k_i) can be obtained from the correlation equation [32]:

$$\frac{k_i d_s}{D_{i,M}} = 2.0 + 0.6 Re^{1/2} Sc^{1/3} \tag{11}$$

where d_s is the diameter of the spherical catalyst pellet, $D_{i,M}$ is the molecular diffusivity of component i, Re is the Reynolds number, and Sc is the Schmidt number.

The diffusion flux of component i ($J_{i,n}$) can be described by the Fick's law:

$$J_{i,n} = -D_{i,e} \frac{dC_{i,n}}{dl_n} \tag{12}$$

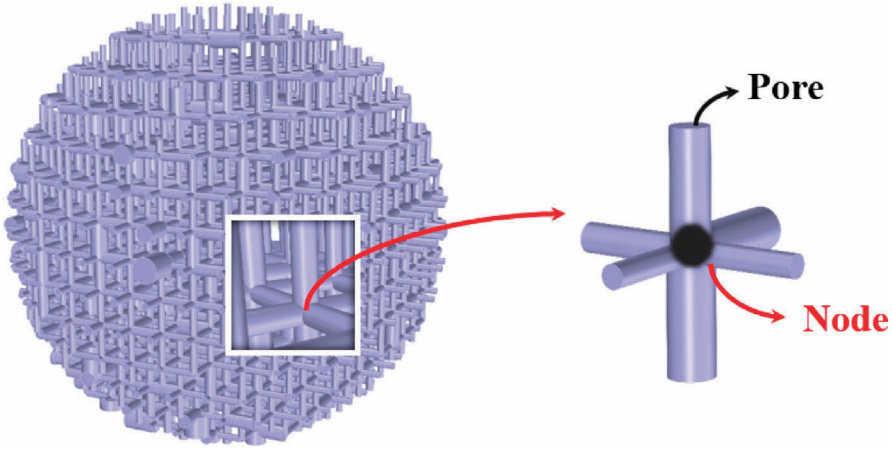

Fig. 1. A typical, spherical pore network used in this work.

$$D_{i,e} = \frac{D_{i,M} D_{i,K}}{D_{i,M} + D_{i,K}} \tag{13}$$

$$D_{i,M} = \frac{1 - x_i}{\sum_{\substack{j=1 \\ j \neq i}}^{n} \frac{x_j}{D_{i,j}}} \tag{14}$$

Here, $D_{i,e}$ is the effective diffusivity of component i and can be obtained by the Wilke-Bosanquet equation [33], $D_{i,M}$ is the molecular diffusion coefficient of component i that can be obtained from the Wilke formula [34], $D_{i,K}$ is the Knudsen diffusivity of component i that is calculated by using the kinetic theory of gases [35]. $D_{i,j}$ is the binary diffusivity of component i in a mixture of i and j, and x_i is the molar fraction of component i. The binary molecular diffusivity ($D_{i,j}$) is determined using the Chapman-Enskog equation [35]:

$$D_{i,j} = \frac{1.8809 \times 10^{-7} \sqrt{T^3 \left(\frac{1}{M_i} + \frac{1}{M_j}\right)}}{P \sigma_{i,j}^2 \Omega_{i,j}} \tag{15}$$

$$\Omega_{i,j} = 1.06036 \left(\frac{\varepsilon_{i,j}}{kT}\right)^{0.15610} + 0.19300 e^{-0.47635 \frac{kT}{\varepsilon_{i,j}}} + 1.03587 e^{-1.52996 \frac{kT}{\varepsilon_{i,j}}} + 1.76474 e^{-3.89411 \frac{kT}{\varepsilon_{i,j}}} \tag{16}$$

$$\sigma_{i,j} = \frac{(\sigma_i + \sigma_j)}{2} \tag{17}$$

$$\varepsilon_{i,j} = \sqrt{\varepsilon_i \varepsilon_j} \tag{18}$$

Here, T is the temperature, M_i is the molecular weight of component i, P is the total pressure, $\sigma_{i,i}$ is the characteristic Lennard-Jones length of component i and j, $\Omega_{i,j}$ is collision integral, and ε_i/k is the characteristic Lennard-Jones energy of component i. The Knudsen diffusivity ($D_{i,K}$) is calculated using the kinetic theory of gases [35]:

$$D_{i,K} = \frac{d_p}{3} \sqrt{\frac{8 R_g T}{\pi M_i}} \tag{19}$$

where R_g is the ideal gas law constant and d_p is the pore diameter.

The reaction kinetics equations for DRM (Eq. (1)) and RWGS (Eq. (2)) are adopted from the work by Richardson and Paripatyadar [36]:

$$R_1 = k_1 \frac{K_{CO_2,1} K_{CH_4,1} P_{CO_2} P_{CH_4}}{S_c (1 + K_{CO_2,1} P_{CO_2} + K_{CH_4,1} P_{CH_4})^2} \left(1 - \frac{P_{CO}^2 P_{H_2}^2}{K_1 P_{CO_2} P_{CH_4}}\right) \tag{20}$$

$$R_2 = k_2 \frac{K_{CO_2,2} K_{H_2,2} P_{CO_2} P_{H_2}}{S_c (1 + K_{CO_2,2} P_{CO_2} + K_{H_2,2} P_{H_2})^2} \left(1 - \frac{P_{CO} P_{H_2O}}{K_2 P_{CO_2} P_{H_2}}\right) \tag{21}$$

Here, R_1 and R_2 are the reaction rates for DRM and RWGS, k_1 and k_2 are the reaction rate constants for DRM and RWGS, $K_{i,1}$ and $K_{i,2}$ are the adsorption equilibrium constants of component i for DRM and RWGS, K_1 and K_2 are the equilibrium constants for DRM and RWGS, S_c is the specific surface area of the DRM catalyst, and P_i is the partial pressure of component i. The reaction rate constants are assumed to be one tenth of the value reported in the literature [36], as the activity of Ni/Al_2O_3 catalyst is around 90% lower than the one of Rh/Al_2O_3 catalyst [17,36]. The other parameters for reaction kinetics are adopted from the same literature [36].

2.3. Equations for coking

Coke can be formed by methane cracking, carbon monoxide disproportionation, and carbon monoxide hydrogenation. The reaction rates for the coking reactions (Eqs. (3)–(5)) are adopted from the work by Snoeck *et al.* [37,38]:

$$R_3 = \frac{k_3 K_{CH_4,3} \left(P_{CH_4} - \frac{P_{H_2}^2}{K_{p_3}}\right)}{\left(1 + K_{CH_4,3} P_{CH_4} + \frac{P_{H_2}^{1.5}}{K_{H_2,3}}\right)^2} \tag{22}$$

$$R_4 = \frac{\frac{k_4}{K_{CO,4} K_{CO_2,4}} \left(\frac{P_{CO_2}}{P_{CO}} - \frac{P_{CO}}{K_{p_4}}\right)}{\left(1 + K_{CO_2,4} P_{CO} + \frac{1}{K_{CO_2,4} K_{CO,4}} \frac{P_{CO_2}}{P_{CO}}\right)^2} \tag{23}$$

$$R_5 = \frac{\frac{k_5}{K_{H_2O,5}} \left(\frac{P_{H_2O}}{P_{H_2}} - \frac{P_{CO}}{K_{p_5}}\right)}{\left(1 + K_{CH_4,5} P_{CH_4} + \frac{1}{K_{H_2O,5}} \frac{P_{H_2O}}{P_{H_2}} + \frac{P_{H_2}^{1.5}}{K_{H_2,5}}\right)^2} \tag{24}$$

Here, k_3, k_4 and k_5 are the reaction rate constants for methane cracking, carbon monoxide disproportionation, and carbon monoxide hydrogenation; K_i (i = CH_4, CO, CO_2, H_2, H_2O) is the adsorption constant for component i; K_{pj} (j = 3, 4, 5) is the equilibrium constant of coking reaction j. The parameters for the coking kinetics are adopted from the same literature [37,38]. The loading of coke in pore n at time $t + \Delta t$ is calculated by:

$$C_{c,n}(t + \Delta t) = C_{c,n}(t) + R_{c,n}(t) \cdot \Delta t \tag{25}$$

In addition, coke deposition can narrow pores, and thus pore diameters in section 2.2 are changed with the loadings of coke. With the assumption of uniform coke distribution on pore surface, the pore diameter of pore n ($d_{p,n}$) can be obtained by:

$$d_{p,n} = \sqrt{d_{0,n}^2 - 4\frac{d_{0,n} \cdot C_{c,n}}{\rho_c}} \tag{26}$$

where $d_{0,n}$ is the initial diameter of pore n and ρ_c is the density of coke. If $d_{p,n}$ is less than the molecular diameter of CH_4 [35] (0.4 nm), the pore n is regarded as a plugged pore. Some pores are not plugged by coke, but surrounded by plugged pores (see Fig. 2). These pores are isolated from reactants, and they are inaccessible pores. An extended Hoshen-Kopelman algorithm is used to identify these inaccessible pores, and the details of this algorithm can be found in the work by Al-Futaisi and Patzek [39].

Coking causes catalyst deactivation mainly in three ways: active site coverage, pore narrowing, and pore blockage. Coke firstly may cover active sites and reduce the catalytic activity. Then, coke can narrow pores and cause the severe diffusion limitation in a catalyst pellet. With the further deposition, coke can even plug some pores and make them completely useless for reaction and diffusion. With the increase of plugged pores, some pores are turned into inaccessible pores that are also unavailable for reaction and diffusion. For DRM catalyzed by Ni/Al_2O_3, filamentous carbon and encapsulated carbon are two major types of coke, and the formation rate of filamentous carbon is much faster than that of encapsulated carbon [40]. Filamentous carbon would not cover Ni sites, and thus the deactivation caused by active site coverage can be assumed to be negligible in this reaction system. In addition, the relation between coke loading and activity has not been reported in the literature for this reaction system. Therefore, only the deactivation caused by pore narrowing and pore blockage is accounted for in this work.

2.4. Implementation

This pore network model is implemented using MATLAB 2021b, and the model parameters are summarized in Table 1. Firstly, the pore network is generated according to the preset structural parameters, including pore size distribution, pore connectivity, and pellet diameter. Then, the model initialization is performed to set initial concentrations and pore states (*i.e.*, accessible, plugged, or inaccessible) in the pore network. After the initialization, the model equations are solved to obtain time-dependent distributions of concentrations, coke loading, and pore states. The equations for diffusion and reaction are solved to yield the concentration profiles in the pore network at time t. With the concentration profiles at time t as input, the coking rates at time t and the coke loadings at time $t + \Delta t$ can be calculated. Using the coke loadings at time $t + \Delta t$, pore diameters and pore states can be updated, and subsequently the equations for diffusion and reaction are solved to obtain the concentration profiles at time $t + \Delta t$. The above calculation steps are repeated until the maximum time for reaction is reached. Finally, the time-dependent distributions of concentrations, coke loading, pore states, and pore network structure are output. The coke content in the catalyst pellet (q_c) can be obtained by:

$$q_c = \frac{S_m}{\sum_{n=1}^{N}(\pi d_{0,n} l_n)} \times \sum_{n=1}^{n=N} \pi d_{0,n} l_n C_{c,n} \tag{27}$$

where S_m is the surface area per unit mass of the catalyst pellet and N is the total number of pores in the pore network. The apparent reaction rate for DRM (R_{app}) is computed using a scaling rule [22,41]:

$$R_{app} = \frac{S_v}{\sum_{n=1}^{N}(\pi d_{0,n} l_n)} \times \sum_{n=1}^{n=N} \pi d_{0,n} l_n R_{CH_4,n} \tag{28}$$

where S_v is the surface area per unit volume of the catalyst pellet. The effectiveness factor of the catalyst pellet (η) is calculated by:

$$\eta = \frac{\sum_{n=1}^{n=N} \pi d_{0,n} l_n R_{CH_4,n}}{R_{CH_4,b} \sum_{n=1}^{n=N} \pi d_{0,n} l_n} \tag{29}$$

where $R_{CH_4,b}$ is the formation rate of CH_4 under the bulk reaction conditions. The coke content, apparent reaction rate, and effectiveness factor are calculated at each time step. These time-dependent q_c, R_{app}, and η are calculated under different reaction conditions and pore network structures, to probe the effects of reaction condition and pore network structure on catalyst deactivation by coking in the DRM reaction.

Table 1
Parameters used in the simulations in this work

Parameter	Value
Reaction time, t/min	0–60
Reaction temperature, T/K	823–973①
Total pressure, P/MPa	0.1–0.5
CH_4/CO_2 molar ratio	0.5–2.0
Pellet radius, R_p/mm	1–4
Pellet porosity, ε	0.5
Support density, ρ_{solid}/kg·m^{-3}	3980②
Coke density, ρ_c/kg·m^{-3}	1200③
Average pore diameter, d_a/nm	2–400
Standard deviation of PSD, σ	0.2–0.8
Pore connectivity, Z	4–8

① Adopted from Cao *et al.* [9].
② Adopted from Yeh and Sacks [42].
③ Adopted from Chua *et al.* [43] and Marin *et al.* [44].

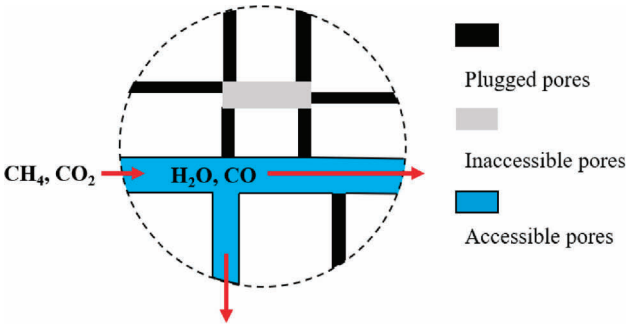

Fig. 2. An illustration of accessible, plugged, and inaccessible pores.

3. Results and Discussion

3.1. Mesh sensitivity analysis

The sensitivity analysis of mesh is performed by comparing four pore networks with different sizes, namely Φ10, Φ14, Φ18, and Φ22, before probing the effects of reaction condition and pore network structure on the catalyst deactivation by coking. The pore network size ΦN means that the diameter of the pore network is the total length of N pores, and the pore length is adjusted to achieve the constant pellet diameter of 2 mm. As seen from Table 2, the total number of pore channels increases from 1662 to 17610

Table 2
Numbers of nodes and pores of the pore networks with different sizes

Pore network size	Total number of nodes	Number of boundary nodes	Number of pores
Φ10	899	414	1662
Φ14	2235	854	4530
Φ18	4463	1466	9654
Φ22	7735	2194	17610

with the pore network size increasing from Φ10 to Φ22. Fig. 3 shows the effects of pore network size on the coke content, apparent reaction rate, and effectiveness factor. The coke content, apparent reaction rate, and effectiveness factor for Φ18 are almost the same as the ones for Φ22, indicating that further increasing pore network size cannot change the simulation results but significantly adds computational cost. Therefore, a pore network size of Φ18 is adequate in this work.

3.2. Effects of reaction conditions

Fig. 4 shows the effect of temperature on the catalyst deactivation by coking. The catalyst pellet is deactivated quickly in this reaction system as indicated in Fig. 4(a). For example, the apparent reaction rate at 823 K approaches 0 (completely deactivation) at the reaction time of 18 min. In addition, increasing the reaction temperature can significantly enhance the initial apparent reaction rate. For example, the initial apparent reaction rate is 703 mol·m^{-3}·s^{-1} at 823 K, and that is 2563 mol·m^{-3}·s^{-1} at 973 K. However, increasing the reaction temperature also makes the catalyst pellet deactivate faster. For example, at 973 K, the time for complete deactivation is only 6 min. Fig. 4(c) gives the time-dependent coke contents under different reaction temperatures. The coke content increases with time before reaching a maximum coke content, which is consistent with the results reported by Gao *et al.* [45]. Increasing the reaction temperature significantly increases the coke formation rate and facilitates catalyst deactivation, although this also increases initial apparent reaction rate. However, the reaction temperature cannot change the maximum coke content as that is primarily determined by the pore network structure of catalyst pellets. In Fig. 4(b), the effectiveness factor decreases with time, as the catalyst pellet is deactivated with time. The initial effectiveness factor decreases from 0.485 to 0.236, with the increase of temperature from 823 to 973 K. At a higher reaction temperature, the intrinsic reaction rate is higher and thus the diffusion limitation in a catalyst pellet is stronger.

Fig. 4(d) displays partial pressures of CH_4 and pore states at the reaction time of 3 min, under the reaction temperatures of 823, 873, 923, and 973 K. The pores in black are the pores completely plugged by coke. The pores in grey are not completely plugged by coke, but they are surrounded by plugged pores and also inaccessible to reactants. The other pores in a color are accessible pores, and the color represents the value of partial pressure of CH_4. At 823 K, some narrow pores are plugged by coke, and inaccessible pores are not observed. At 873 K, the number of plugged pores increases a lot, and some inaccessible pores are found. At 923 K, most of the pores are plugged or inaccessible pores. At 973 K, almost all the pores are unavailable for diffusion and reaction, and the catalyst pellet is close to complete deactivation. At a higher reaction temperature, the formation rate of coke is larger, and pores are easily occupied by coke. Thus, more plugged and inaccessible pores are observed at a higher reaction temperature.

Fig. 5(a)–(c) present the time-dependent apparent reaction rates (R_{app}), effectiveness factors (η), and coke contents (q_c), under different total pressures. With the increase of total pressure from 0.1 to 0.5 MPa, the initial apparent reaction rate increases from 703 mol·m^{-3}·s^{-1} to 1072 mol·m^{-3}·s^{-1}. This result is expected, as the intrinsic reaction rate increases with total pressure. The catalyst deactivation becomes faster with the increase of total pressure. For example, the time for complete catalyst deactivation is 20 min for $P = 0.1$ MPa, while that is 9 min for $P = 0.5$ MPa. The formation rate of coke increases with the total pressure, resulting in the faster catalyst deactivation at a higher total pressure. Fig. 5(b) shows that the effectiveness factor decreases with the increase of total pressure at a reaction time, as the intrinsic reaction rate is higher and thus the diffusion limitation is stronger at a higher total pressure. In Fig. 5(c), the maximum coke contents under different total pressures are almost the same, although the apparent coking rate increases with the total pressure. This result indicates that the maximum coke content is independent of the total pressure.

Fig. 5(d) displays partial pressures of CH_4 and pore states at the reaction time of 6 min, under different total pressures. With the increase of total pressure, the number of plugged and inaccessible pores goes up largely. As the formation rate of coke at a higher total pressure is larger, the pore network is easier to be occupied by coke. A higher total pressure is favorable in increasing the production rate of syngas and thus in reducing reactor volume, but it also makes the catalyst pellet more vulnerable to coking. Therefore, an optimal total pressure should balance these factors.

Fig. 6 shows how the molar ratio of CH_4 to CO_2 in the bulk (CH_4/CO_2) affects the catalyst deactivation by coking. As seen from Fig. 6(a), the initial apparent reaction rate decreases from 708 mol·m^{-3}·s^{-1} to 556 mol·m^{-3}·s^{-1} with the increases of CH_4/CO_2 from 0.5 to 2. This result can be explained by analyzing the reaction kinetics. The adsorption constant for CH_4 is larger than that of CO_2, and thus the intrinsic reaction rate decreases with the increase of CH_4/CO_2 under the constant total pressure of 0.1 MPa. The catalyst deactivation becomes faster with the increase of CH_4/CO_2. For example, the reaction time for complete deactivation is 48 min for $CH_4/CO_2 = 0.5$, while that is 12 min for $CH_4/CO_2 = 2$. A lower CH_4/CO_2 means a higher partial pressure of CO_2. More CO_2 in this reaction system is better in promoting the

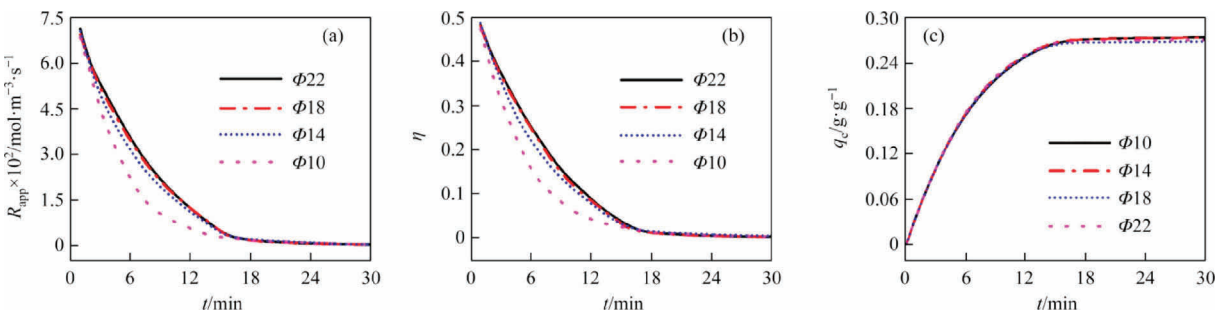

Fig. 3. Time-dependent (a) apparent reaction rates (R_{app}), (b) effectiveness factors (η), and (c) coke contents (q_c) under different pore network sizes. Simulation parameters: $T = 823$ K, $P = 0.1$ MPa, $CH_4/CO_2 = 1$, $d_a = 10$ nm, $\sigma = 0.5$, $Z = 6$ and $R_p = 1$ mm. The other parameters are given in Table 1.

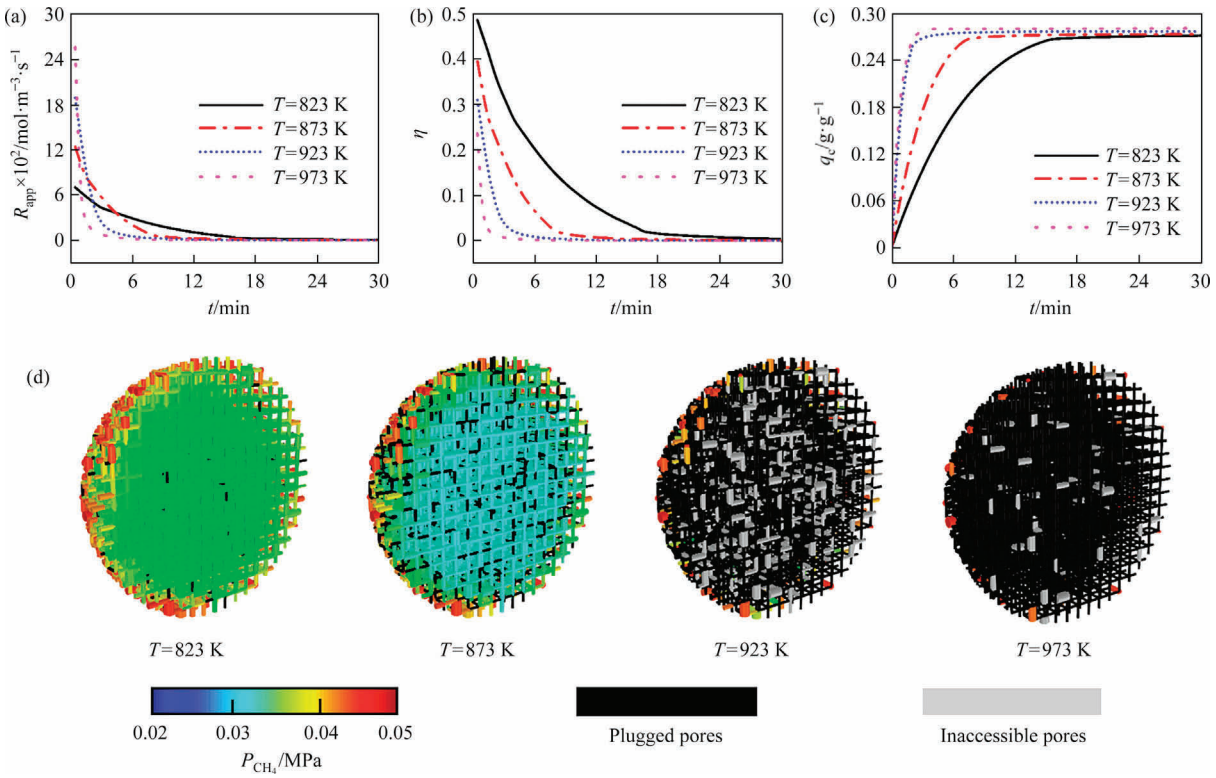

Fig. 4. Time-dependent (a) apparent reaction rates (R_{app}), (b) effectiveness factors (η) and (c) coke contents (q_c), and (d) pore states at t = 3 min, under different reaction temperatures (T). Simulation parameters: P = 0.1 MPa, CH_4/CO_2 = 1, d_a = 10 nm, σ = 0.5, Z = 6 and R_p = 1 mm. The other parameters are given in Table 1.

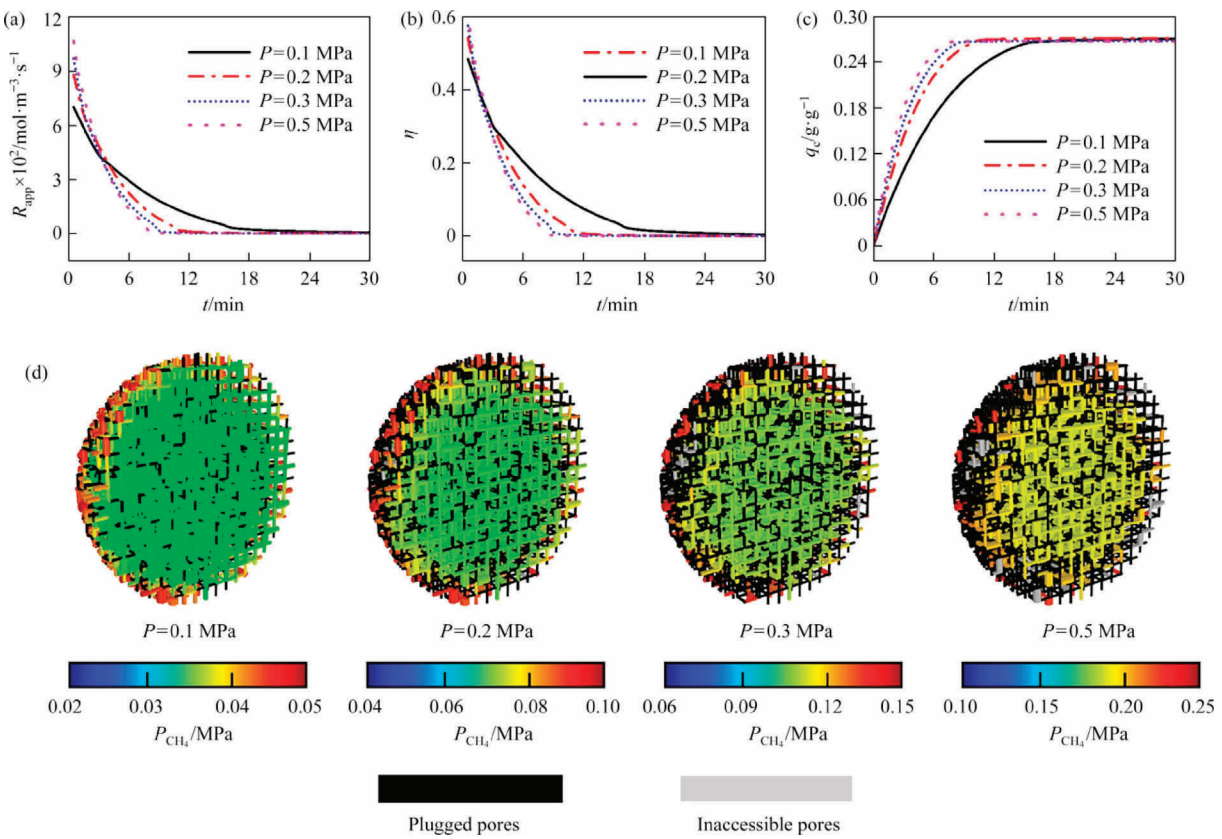

Fig. 5. Time-dependent (a) apparent reaction rates (R_{app}), (b) effectiveness factors (η) and (c) coke contents (q_c), and (d) pore states at t = 6 min, under different total pressures (P). Simulation parameters: T = 823 K, CH_4/CO_2 = 1, d_a = 10 nm, σ = 0.5, Z = 6 and R_p = 1 mm. The other parameters are given in Table 1.

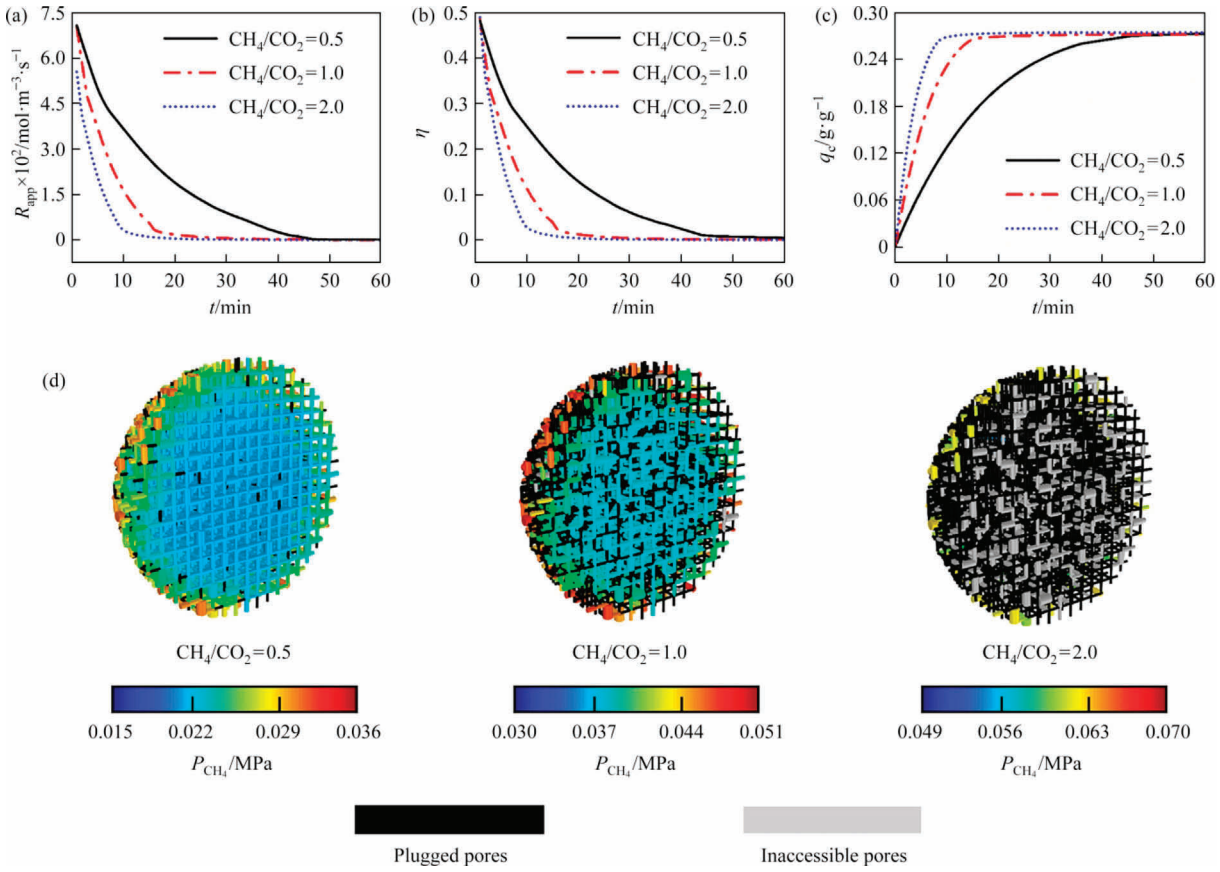

Fig. 6. Time-dependent (a) apparent reaction rates (R_{app}), (b) effectiveness factors (η) and (c) coke contents (q_c), and (d) pore states at $t = 10$ min, under different molar ratios of CH_4 to CO_2 in the bulk (CH_4/CO_2). Simulation parameters: $T = 823$ K, $P = 0.1$ MPa, $d_a = 10$ nm, $\sigma = 0.5$, $Z = 6$ and $R_p = 1$ mm. The other parameters are given in Table 1.

reaction of RWGS to produce more H_2O and CO. With the increase of H_2O in the catalyst pellet, coke becomes easier to be gasified, and thus the apparent coke formation rate decreases with the decrease of CH_4/CO_2. In Fig. 6(b), the initial effectiveness factors at $CH_4/CO_2 = 0.5$, 1, and 2 are almost the same. At a lower CH_4/CO_2, the intrinsic reaction rate is higher, but the diffusion of CH_4 is slower; at a higher CH_4/CO_2, the intrinsic reaction rate is lower, but the diffusion of CH_4 is faster. Thus, the two competing factors lead to the similar effectiveness factors under different CH_4/CO_2. In Fig. 6(c), the maximum coke contents are almost the same under different CH_4/CO_2, although the apparent coking rate increases with CH_4/CO_2. This result clearly indicates that the maximum coke content does not change with the molar ratio of CH_4 to CO_2. As seen from Fig. 6(d), the number of plugged and inaccessible pores increases with CH_4/CO_2 at the reaction time of 10 min. These results show that a higher proportion of CO_2 in the feed should be favorable in reducing the coking rate and prolonging the catalyst lifetime, which has been observed in experiments [46].

3.3. Effects of pore network structure

Fig. 7 shows how the volume-averaged pore diameter (d_a) affects the catalyst deactivation by coking. The apparent reaction rate (R_{app}) at $t = 0$ increases from 181 mol·m^{-3}·s^{-1} to 1447 mol·m^{-3}·s^{-1}, with the volume-averaged pore diameter changing from 2 to 400 nm. A larger pore diameter indicates weaker resistance for diffusion, and a higher effectiveness factor. For example, the initial effectiveness factor for $d_a = 2$ nm is only 0.125, while that for $d_a = 50$ nm approaches 1 (see Fig. 7(b)). The catalyst deactivation becomes slower with the increase of volume-averaged pore diameter. For instance, the reaction time for complete catalyst deactivation is 5 min for $d_a = 2$ nm, while R_{app} for $d_a = 400$ nm only decreases by 7.04% after 60 min on stream. Obviously, the catalyst pellet with larger pores is more robust against catalyst deactivation by coking. A large pore is not easily plugged by coke, and thus the catalyst pellet with large pores has a good stability. This result is similar to the one obtained from experiments [47]. Fig. 7(c) shows that the maximum coke contents for $d_a = 2$ and 10 nm are almost the same. This is because all the catalysts have the same pore volume. The catalysts with $d_a = 50$ and 400 nm do not reach a maximum coke content within 60 min on stream. Fig. 7(d) displays partial pressures of CH_4 and pore states at the reaction time of 10 min under the volume-averaged pore diameters of 2, 10, 50, and 400 nm. For $d_a = 2$ nm, almost all the pores are plugged or inaccessible, and the catalyst is completely deactivated; for $d_a = 10$ nm, some pores are still available for diffusion and reaction; for $d_a = 50$ and 400 nm, almost all the pores are available, although the coke layer has formed on pore surface. These results show that the catalyst pellet with a large pore diameter is favorable for DRM: the diffusion limitation is weak, on the one hand; the catalyst is robust against catalyst deactivation by coking, on the other hand.

Fig. 8 displays the effect of standard deviation of pore size distribution (σ) on the catalyst deactivation by coking. As seen from Fig. 8(a), the initial apparent reaction rate decreases from 907 mol·m^{-3}·s^{-1} to 452 mol·m^{-3}·s^{-1}, when changing the standard deviation from 0.2 to 0.8. A higher standard deviation means the pore size distribution is wide, and the pore network is more tortuous. A tortuous pore network is not favorable for diffusion, which results in the lower initial apparent reaction rate for a higher standard deviation. The reaction times for complete deactivation for σ =0.2, 0.4, 0.6, and 0.8 are close. For the catalyst pel-

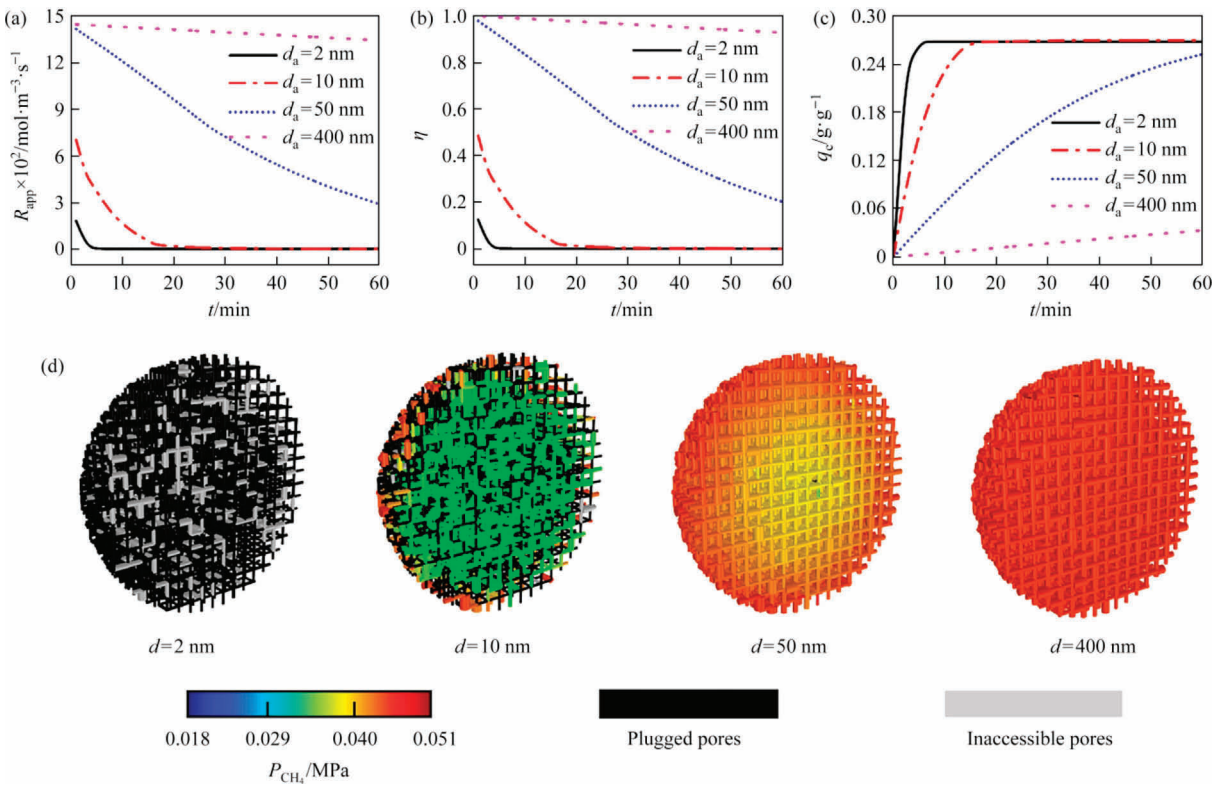

Fig. 7. Time-dependent (a) apparent reaction rates (R_{app}), (b) effectiveness factors (η) and (c) coke contents (q_c), and (d) pore states at $t = 10$ min, under different volume-averaged pore diameters (d_a). Simulation parameters: $T = 823$ K, $P = 0.1$ MPa, $CH_4/CO_2 = 1$, $\sigma = 0.5$, $Z = 6$ and $R_p = 1$ mm. The other parameters are given in Table 1.

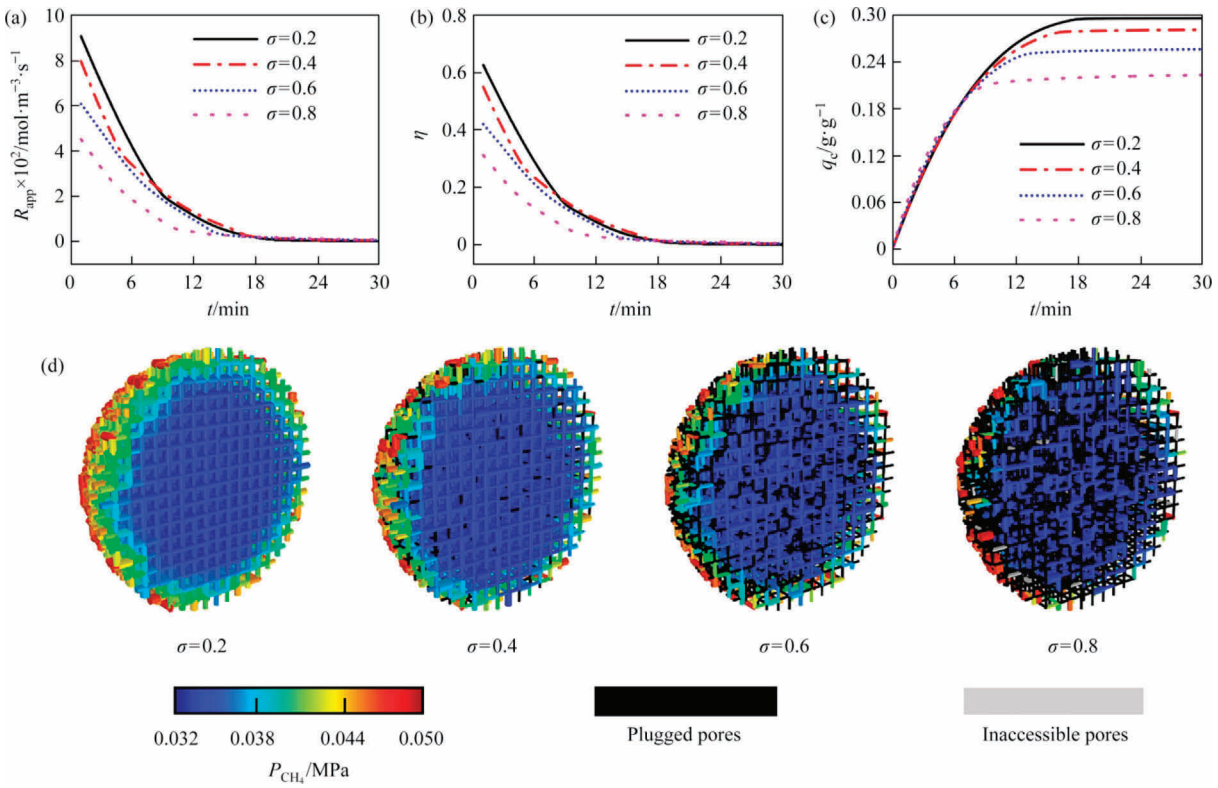

Fig. 8. Time-dependent (a) apparent reaction rates (R_{app}), (b) effectiveness factors (η) and (c) coke contents (q_c), and (d) pore states at $t = 6$ min, under different standard deviations of pore size distribution (σ). Simulation parameters: $T = 823$ K, $P = 0.1$ MPa, $CH_4/CO_2 = 1$, $d_a = 10$ nm, $Z = 6$ and $R_p = 1$ mm. The other parameters are given in Table 1.

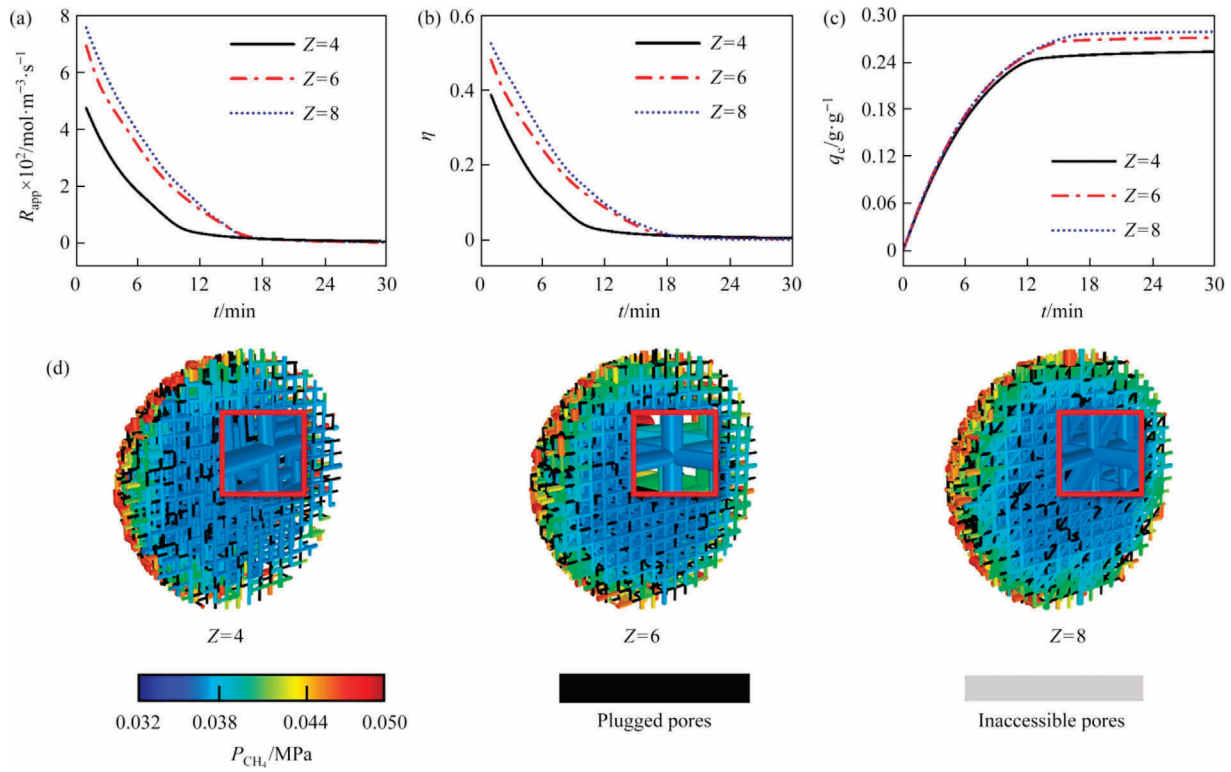

Fig. 9. Time-dependent (a) apparent reaction rates (R_{app}), (b) effectiveness factors (η) and (c) coke contents (q_c), and (d) pore states at $t = 6$ min, under different pore connectivities (Z). Simulation parameters: $T = 823$ K, $P = 0.1$ MPa, $CH_4/CO_2 = 1$, $d_a = 10$ nm, $\sigma = 0.5$ and $R_p = 1$ mm. The other parameters are given in Table 1.

let with a large σ, the pore size is widely dispersed, containing a number of both narrow pores and wide pores. Narrow pores are easily plugged by coke and become completely deactivated; wide pores can contain much coke and are robust against catalyst deactivation by coking. In Fig. 8(c), the apparent coke formation rates for σ =0.2, 0.4, 0.6, and 0.8 are very close, indicating the coking rate would not be significantly affected by the standard deviation of pore size distribution. Fig. 8(c) also shows that the maximum coke content increases from 0.2248 to 0.2956 g·g^{-1} with the increase of standard deviation from 0.2 to 0.8. A wider pore size distribution means more narrow pores, the narrow pores are plugged by coke quickly. Then these plugged narrow pores would isolate wide pores and make them unavailable for DRM and coking reactions. But, for the catalyst pellet with a narrower pore size distribution, the pores are more uniformly covered by coke. Thus, the maximum coke content for a narrower pore size distribution is larger. Fig. 8(d) displays partial pressures of CH_4 and pore states at the reaction time of 6 min. The number of plugged pores increases with the standard deviation. This is because the pore network with a larger standard deviation contains more narrow pores and narrow pores are easily plugged by coke. Generally, the catalyst pellet with a narrow pore size distribution should be better, as the diffusion limitation is weaker and the pore network can contain more coke.

Fig. 9 presents the effect of pore connectivity (Z) on the catalyst deactivation by coking. As seen from Fig. 9(a), the initial apparent reaction rate increases from 476 mol·m^{-3}·s^{-1} to 759 mol·m^{-3}·s^{-1} with the increase of pore connectivity from 4 to 8. The pores are better connected with a larger pore connectivity, indicating the diffusion limitation is weaker. The effectiveness factor decreases with the increase of pore connectivity, which also confirms the reduced diffusion limitation with pore connectivity. The pore network with a larger pore connectivity is more robust against catalyst deactivation by coking. For example, the reaction time for complete deactivation for $Z = 4$ is 10 min, while that for $Z = 6$ is 18 min. Fig. 9(c) shows that the pore network with a larger pore connectivity has a larger maximum coke content. For instance, the maximum coke content for $Z = 4$ is 0.2547 g·g^{-1}, while that for $Z = 8$ is 0.2796 g·g^{-1}. For a poorly connected pore network, some wide pores are more easily isolated by plugged narrow pores. Obvious, the catalyst pellet with a well-connected pore network is more favorable, as the diffusion limitation is weaker and the pore network can contain more coke.

Fig. 10 shows the effect of pellet radius (R_p) on the catalyst deactivation by coking. As seen from Fig. 10(a), the initial apparent reaction rate decreases from 703 mol·m^{-3}·s^{-1} to 187 mol·m^{-3}·s^{-1} with the increase of pellet radius from 1.0 mm to 4.0 mm. This result is expected, as a larger catalyst pellet has a longer diffusion path length. The effectiveness factor in Fig. 10(b) decreases with the increase of pellet radius, as the diffusion limitation becomes stronger. Besides, the coke content curves in Fig. 10(c) are very close for different pellet radii. According to Eqs. (3)–(5) and (22)–(24), both reactant (CH_4) and products (CO and H_2) are coke precursors, and they all affect the coking rate. The total concentration of coke precursors does not change largely with pellet radius, which explains the close coking rates and then coke contents. Fig. 10(d) shows partial pressures of CH_4 and pore states at the reaction time of 6 min. The concentration gradient for R_p = 1 mm is the lowest, due to its shortest diffusion path length. Generally, the catalyst pellet with a small size is favorable in enhancing its apparent catalytic activity without significantly changing its deactivation by coking.

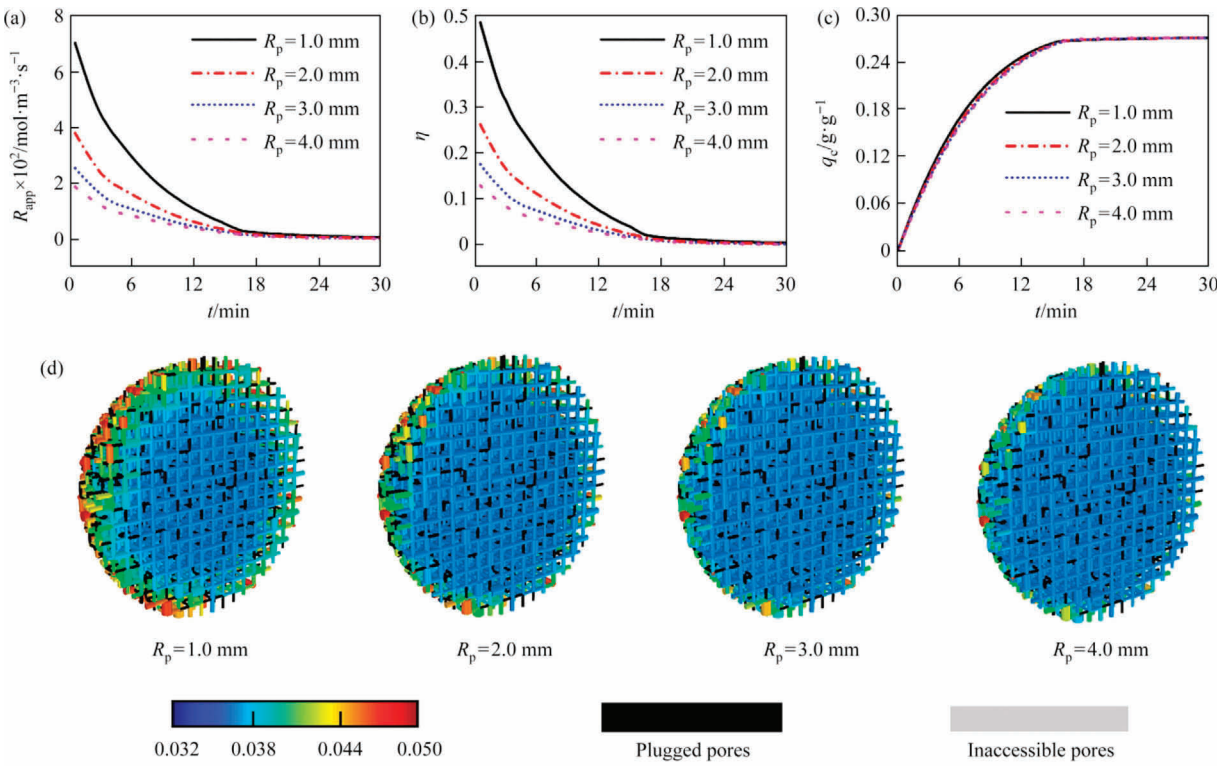

Fig. 10. Time-dependent (a) apparent reaction rates (R_{app}), (b) effectiveness factors (η) and (c) coke contents (q_c), and (d) pore states at $t = 6$ min, under different pellet radii (R_p). Simulation parameters: $T = 823$ K, $P = 0.1$ MPa, $CH_4/CO_2 = 1$, $d_a = 10$ nm, $\sigma = 0.5$ and $Z = 6$. The other parameters are given in Table 1.

4. Conclusions

In this work, a pore network is proposed to probe the catalyst deactivation by coking in Ni/Al_2O_3 catalyst pellets for dry reforming of methane (DRM). This pore network can well describe the pore structure in catalyst pellets and the pore blockage caused by coke. The effects of reaction conditions (*i.e.*, temperature, pressure, and CH_4/CO_2 molar ratio) and pore structure (*i.e.*, pore diameter, pore size distribution, and pore connectivity) on the catalyst deactivation by coking are investigated using this pore network model.

The results show that reaction temperature, total pressure, and CH_4/CO_2 molar ratio can significantly affect the catalyst deactivation by coking. Under a lower reaction temperature, a lower total pressure, and a smaller CH_4/CO_2 molar ratio, the catalyst deactivation by coking is slower, as the coke formation rate is lower. The maximum coke content in a DRM catalyst pellet is independent of these reaction conditions. Pore network structure can also largely change the catalyst deactivation by coking. The DRM catalyst pellet with a larger pore diameter, a narrower pore size distribution and a larger pore connectivity is more robust against catalyst deactivation by coking, as the pores are more difficult to be plugged or inaccessible. With a fixed pore volume, the catalyst pellet with a narrower pore size distribution and a larger pore connectivity can contain more coke. Besides, catalyst pellet radius only slightly changes the coke content, although a smaller pellet radius shows a higher apparent reaction rate due to the shorter diffusion path length. The pore network model and results in this work should be used in the optimal design of DRM catalyst pellets, and some other industrial catalyst pellets with deactivation by coking.

Declaration of Competing Interest

The authors declare that they have no known competing financial interests or personal relationships that could have appeared to influence the work reported in this paper.

Acknowledgements

This work was financially supported by the National Natural Science Foundation of China (22078090 and 92034301), the Shanghai Rising-Star Program (21QA1402000), the Natural Science Foundation of Shanghai (21ZR1418100), and the Open Project of State Key Laboratory of Chemical Engineering (SKL-ChE-21C02).

References

[1] S. Hallegatte, J. Rogelj, M. Allen, L. Clarke, O. Edenhofer, C.B. Field, P. Friedlingstein, L. Van Kesteren, R. Knutti, K.J. Mach, M. Mastrandrea, A. Michel, J. Minx, M. Oppenheimer, G.K. Plattner, K. Riahi, M. Schaeffer, T.F. Stocker, D.P. Van Vuuren, Mapping the climate change challenge, *Nat. Clim. Chang.* 6 (7) (2016) 663–668.
[2] D.Y.C. Leung, G. Caramanna, M.M. Maroto-Valer, An overview of current status of carbon dioxide capture and storage technologies, *Renew. Sustain. Energy Rev.* 39 (2014) 426–443.
[3] R. Kotagodahetti, K. Hewage, H. Karunathilake, R. Sadiq, Evaluating carbon capturing strategies for emissions reduction in community energy systems: A life cycle thinking approach, *Energy* 232 (2021) 121012.
[4] J.M. Lavoie, Review on dry reforming of methane, a potentially more environmentally-friendly approach to the increasing natural gas exploitation, *Front. Chem.* 2 (2014) 81.
[5] G. Zhang, J. Liu, Y. Xu, Y. Sun, A review of CH_4–CO_2 reforming to synthesis gas over Ni-based catalysts in recent years (2010–2017), *Int. J. Hydrogen Energy.* 43 (32) (2018) 15030–15054.
[6] D. Pakhare, J. Spivey, A review of dry (CO_2) reforming of methane over noble metal catalysts, *Chem. Soc. Rev.* 43 (22) (2014) 7813–7837.
[7] W. Schakel, G. Oreggioni, B. Singh, A. Strømman, A. Ramírez, Assessing the techno-environmental performance of CO_2 utilization *via* dry reforming of methane for the production of dimethyl ether, *J. CO_2 Util.* 16 (2016) 138–149.
[8] Q.Q. Chen, D.F. Wang, Y. Gu, S. Yang, Z.Y. Tang, Y.H. Sun, Q. Wu, Techno-economic evaluation of CO_2-rich natural gas dry reforming for linear alpha olefins production, *Energy Convers. Manag.* 205 (2020) 112348.
[9] P.F. Cao, S. Adegbite, T. Wu, Thermodynamic equilibrium analysis of CO_2 reforming of methane: Elimination of carbon deposition and adjustment of H_2/CO ratio, *Energy Procedia* 105 (2017) 1864–1869.
[10] Z.L. Zhang, X.E. Verykios, Carbon dioxide reforming of methane to synthesis gas over Ni/La_2O_3 catalysts, *Appl. Catal. A Gen.* 138 (1) (1996) 109–133.
[11] J.M. Ginsburg, J. Piña, T. El Solh, H.I. de Lasa, Coke formation over a nickel catalyst under methane dry reforming conditions: Thermodynamic and kinetic models, *Ind. Eng. Chem. Res.* 44 (14) (2005) 4846–4854.

[12] O. Muraza, A. Galadima, A review on coke management during dry reforming of methane, *Int. J. Energy Res.* 39 (9) (2015) 1196–1216.
[13] P.J. Megía, A.J. Vizcaíno, M. Ruiz-Abad, J.A. Calles, A. Carrero, Coke evolution in simulated bio-oil aqueous fraction steam reforming using Co/SBA-15, *Catal. Today* 367 (2021) 145–152.
[14] E. Rodríguez, G. Félix, J. Ancheyta, F. Trejo, Modeling of hydrotreating catalyst deactivation for heavy oil hydrocarbons, *Fuel* 225 (2018) 118–133.
[15] Y.S. Zhang, X.K. Lu, R.E. Owen, G. Manos, R.Y. Xu, F.R. Wang, W.C. Maskell, P.R. Shearing, D.J.L. Brett, Fine structural changes of fluid catalytic catalysts and characterization of coke formed resulting from heavy oil devolatilization, *Appl. Catal. B Environ.* 263 (2020) 118329.
[16] S. Sokolov, E.V. Kondratenko, M.M. Pohl, U. Rodemerck, Effect of calcination conditions on time on-stream performance of Ni/La_2O_3-ZrO_2 in low-temperature dry reforming of methane, *Int. J. Hydrog. Energy* 38 (36) (2013) 16121–16132.
[17] W.Y. Kim, Y.H. Lee, H. Park, Y.H. Choi, M.H. Lee, J.S. Lee, Coke tolerance of Ni/Al_2O_3 nanosheet catalyst for dry reforming of methane, *Catal. Sci. Technol.* 6 (7) (2016) 2060–2064.
[18] J.S. Zhang, F.X. Li, Coke-resistant Ni@SiO_2 catalyst for dry reforming of methane, *Appl. Catal. B Environ.* 176–177 (2015) 513–521.
[19] M. Németh, G. Sáfrán, A. Horváth, F. Somodi, Hindered methane decomposition on a coke-resistant Ni-In/SiO_2 dry reforming catalyst, *Catal. Commun.* 118 (2019) 56–59.
[20] J. Jeon, S. Nam, C.H. Ko, Rapid evaluation of coke resistance in catalysts for methane reforming using low steam-to-carbon ratio, *Catal. Today* 309 (2018) 140–146.
[21] F.J. Keil, C. Rieckmann, Optimization of catalytic pore structures, *Hungarian J. Ind. Chem.* 21 (1993) 277–286.
[22] F.J. Keil, C. Rieckmann, Optimization of three-dimensional catalyst pore structures, *Chem. Eng. Sci.* 49 (24) (1994) 4811–4822.
[23] G.H. Ye, H.Z. Wang, X.G. Zhou, F.J. Keil, M.O. Coppens, W.K. Yuan, Optimizing catalyst pore network structure in the presence of deactivation by coking, *Aiche J.* 65 (10) (2019) e16687.
[24] G.H. Ye, H.Z. Wang, X.Z. Duan, Z.J. Sui, X.G. Zhou, M.O. Coppens, W.K. Yuan, Pore network modeling of catalyst deactivation by coking, from single site to particle, during propane dehydrogenation, *AIChE J.* 65 (1) (2019) 140–150.
[25] I.V. Zenyuk, E. Medici, J. Allen, A.Z. Weber, Coupling continuum and pore-network models for polymer-electrolyte fuel cells, *Int. J. Hydrog. Energy* 40 (46) (2015) 16831–16845.
[26] X.L. Liu, Q.F. Zhang, G.H. Ye, J.J. Li, P. Li, X.G. Zhou, F.J. Keil, Deactivation and regeneration of Claus catalyst particles unraveled by pore network model, *Chem. Eng. Sci.* 211 (2020) 115305.
[27] G.H. Ye, Y.Y. Sun, X.G. Zhou, K.K. Zhu, J.H. Zhou, M.O. Coppens, Method for generating pore networks in porous particles of arbitrary shape, and its application to catalytic hydrogenation of benzene, *Chem. Eng. J.* 329 (2017) 56–65.
[28] Z.M. Zhou, Z.M. Cheng, Z. Li, W.K. Yuan, Determination of effectiveness factor of a partial internal wetting catalyst from adsorption measurement, *Chem. Eng. Sci.* 59 (20) (2004) 4305–4311.
[29] J.S.S. Mohammadzadeh, A. Zamaniyan, Catalyst shape as a design parameter—Optimum shape for methane-steam reforming catalyst, *Chem. Eng. Res. Des.* 80 (4) (2002) 383–391.
[30] A. Zamaniyan, A.A. Khodadadi, Y. Mortazavi, H. Manafi, Comparative model analysis of the performance of tube fitted bulk monolithic catalyst with conventional pellet shapes for natural gas reforming, *J. Ind. Eng. Chem.* 17 (4) (2011) 767–776.
[31] J.A. Calles, A. Carrero, A.J. Vizcaíno, P.J. Megía, Agglomerated Co-Cr/SBA-15 catalysts for hydrogen production through acetic acid steam reforming, *Int. J. Hydrog. Energy* 45 (32) (2020) 15941–15950.
[32] N. Wakao, T. Funazkri, Effect of fluid dispersion coefficients on particle-to-fluid mass transfer coefficients in packed beds: Correlation of Sherwood numbers, *Chem. Eng. Sci.* 33 (10) (1978) 1375–1384.
[33] R. Krishna, J.A. Wesselingh, The Maxwell-Stefan approach to mass transfer, *Chem. Eng. Sci.* 52 (6) (1997) 861–911.
[34] D.F. Fairbanks, C.R. Wilke, Diffusion coefficients in multicomponent gas mixtures, *Ind. Eng. Chem.* 42 (3) (1950) 471–475.
[35] B.E. Poling, J.M. Prausnitz, J.P. O'Connell, The Properties of Gases and Liquids, 5th Ed., McGraw-Hill, New York, 2000.
[36] J.T. Richardson, S.A. Paripatyadar, Carbon dioxide reforming of methane with supported rhodium, *Appl. Catal.* 61 (1) (1990) 293–309.
[37] J.W. Snoeck, G.F. Froment, M. Fowles, Filamentous carbon formation and gasification: Thermodynamics, driving force, nucleation, and steady-state growth, *J. Catal.* 169 (1) (1997) 240–249.
[38] J.W. Snoeck, G.F. Froment, M. Fowles, Steam/CO_2 reforming of methane carbon formation and gasification on catalysts with various potassium contents, *Ind. Eng. Chem. Res.* 41 (15) (2002) 3548–3556.
[39] A. Al-Futaisi, T.W. Patzek, Extension of Hoshen-Kopelman algorithm to non-lattice environments, *Phys. A Stat. Mech. Appl.* 321 (3–4) (2003) 665–678.
[40] J.R. Rostrup-Nielsen, J. Sehested, J.K. Nørskov, Hydrogen and synthesis gas by steam- and CO_2 reforming, *Adv. Catal.* 47 (2002) 65–139.
[41] F.J. Keil, Diffusion and reaction in porous networks, *Catal. Today* 53 (2) (1999) 245–258.
[42] T.S. Yeh, M.D. Sacks, Effect of particle size distribution on the sintering of alumina C–484 *J. Am. Ceram. Soc.* 71 (12) (1988) C-484–C-487.
[43] L.M. Chua, T. Vazhnova, T.J. Mays, D.B. Lukyanov, S.P. Rigby, Deactivation of PtH-MFI bifunctional catalysts by coke formation during benzene alkylation with ethane, *J. Catal.* 271 (2) (2010) 401–412.
[44] G.B. Marin, J.W. Beeckman, G.F. Froment, Rigorous kinetic models for catalyst deactivation by coke deposition: Application to butene dehydrogenation, *J. Catal.* 97 (2) (1986) 416–426.
[45] M.B. Gao, H. Li, M. Yang, J.B. Zhou, X.S. Yuan, P. Tian, M. Ye, Z.M. Liu, A modeling study on reaction and diffusion in MTO process over SAPO-34 zeolites, *Chem. Eng. J.* 377 (2019) 119668.
[46] D.L. Li, Y. Nakagawa, K. Tomishige, Methane reforming to synthesis gas over Ni catalysts modified with noble metals, *Appl. Catal. A Gen.* 408 (1–2) (2011) 1–24.
[47] E.L.G. Oliveira, C.A. Grande, A.E. Rodrigues, Methane steam reforming in large pore catalyst, *Chem. Eng. Sci.* 65 (5) (2010) 1539–1550.